Author Accepted Manuscript – Formal publication: https://doi.org/10.1016/j.est.2020.101684

A support approach for the modular design of Li-ion batteries: a test case with PCM

Paolo Cicconi[1*], Pradeep Kumar[2], Peeyush Varshney[2]

[1] *Università degli Studi Roma Tre, Rome, Italy.*
[2] *Zakir Husain College of Engineering and Technology, Aligarh Muslim University, Aligarh, India.*

*corresponding author: Paolo Cicconi, paolo.cicconi@uniroma3.it

ABSTRACT:

Nowadays, there is an increasing interest in Phase-Change Materials due to their capacity to store latent heat during the phase transition. In the literature, the solid-liquid change is widely applied in cooling applications such as the thermal management of Li-ion batteries. The optimization of the cooling system is one of the solutions to reduce battery aging and increase the battery lifetime. Even if Phase-Change Materials are studied to be used in this context, there is still a lack of suitable solutions to be used in engineering design for a further product commercialization. In this context, the paper proposes a modular approach to support the design of a battery pack considering Phase-Change Materials in the cooling system. The approach shows how a single module of cells can be stacked and how the cooling system of each module can be easily connected to each other. The modularity concept is extended from the electrical configuration to the cooling system. As a test case, a battery module has been analyzed. The battery module has been simulated using a Computer-Aided Engineering tool to analyze the behavior of the temperature profile under loading conditions.

Keywords: Phase-Change Materials (PCM); Li-ion batteries; Modular design; Battery simulations; Battery cooling; Battery Thermal Management.

Author Accepted Manuscript – Formal publication: https://doi.org/10.1016/j.est.2020.101684

1 INTRODUCTION

Low and high values of temperature can reduce battery health and lifecycle [1]. As a solution, a lot of scholars have been testing Phase-Change Materials (PCM) for the thermal management of Li-ion batteries [2] [3] [4]. These materials can absorb energy without increasing their temperature during the phase-change. PCM materials are particularly attractive and chosen as one of the most interesting cooling options in terms of their high-energy storage density [5]. Moreover, they are also less complex and expensive than traditional cooling methods (liquid cooling, air forced fan, etc.) [6]. In general, the applications of PCM materials not only regard automotive [1], but also PV solar systems [7] [8], building [9], energy management systems for building [10] [11] [12] [13], etc. Focusing on applications for batteries, even if these materials are cost-effective, their employment in commercial solutions is still limited to problems such as the volume change [14] and the difficult to exchange the heat which is released after the phase-change [15].

The design of a battery pack regards a complex activity which has to consider several aspects such as safety [3] and reliability while reducing the relative life cycle cost [16]. The cooling technology is very important to reduce the negative influence of temperature [17], to improve the safety in use, and to improve the battery efficiency by reducing the aging rate [18]. In this context, the thermal analysis is very important to evaluate the operation of the battery pack [19]. However, the simulation of the temperature behavior in Li-ion batteries needs of tools to analyze the complexity of the temperature inconsistency in operation [20].

The reduction of cost and lead-time is an important target in battery design for automotive [20]. The integration between the study of the battery layout, the thermal simulations, and the cost analysis needs efficient design tools and methods to improve the engineering activity. This issue is more evident in the design of customized solutions for small-batches production. Configurations and simulations have been already applied in past works to reduce cost and time in the design of battery packs [21]. As an example, Pelletier et al. presented a design framework bases on the solution of a Constraints Satisfaction Problem

Author Accepted Manuscript – Formal publication: https://doi.org/10.1016/j.est.2020.101684

(CSP) model [22]. A lot of the past studies are focused on traditional schemes of battery layout. However, the design of battery packs requires the definition of novel configurations because a reference standard still does not exist. As an answer, Qian et al. proposed an innovative layout to optimize the cooling performance in a battery module with 18650 cells [23]. The design of battery packs requires the study of innovative solutions to improve the cooling system and the behavior of the Battery Thermal Management System (BTMS).

This paper shows a modular approach to support the design of Li-ion batteries including the employment of PCM. The design of the cooling system is defined within the modularization concept. As a test case, the paper proposes the study of a new cooling layout for Li-ion batteries used for energy storage applications. The analyzed battery consists of modules with 18 cylindrical-NMC cells. The battery module is the smaller operative unit that includes its cooling system. A modularization approach is introduced during the design activity to achieve important targets in terms of assembly and thermal management. Here modularity is proposed as a key to reducing cost and increasing battery performance. The novelty regards the combination of a modular cooling into a battery module including PCM material and air-cooling system.

This paper is organized into seven sections. Section 3 describes the methodological approach for the design of a battery module with a modular cooling system which includes the use of PCM materials. A test case with cylindrical Li-ion cells is described in Section 4, and the results are given in Section 5. Finally, discussion and conclusions are reported in Section 6 and Section 7 at the end of the paper.

2 Research background on battery cooling and PCM

Focusing on the design of Li-ion batteries, several studies are proposed in the literature to improve the efficiency and performance of the cooling system. Different cooling strategies can be used to enhance the thermal performance of the battery pack. The selection of the cooling method depends upon various parameters like environmental conditions, size of the battery pack, etc. In order to control the thermal performance of Li-ion battery packs, it becomes necessary to select an efficient cooling system for the battery pack.

Pesaran et al.[24] studied the effect of air-cooling on the thermal performance of the battery pack. The parallel airflow approach was followed to study the lumped capacitance battery thermal model in Matlab to monitor the thermal performance of the battery pack. Giuliano et al [25] studied the use of metal foam-based heat exchanger plates with an air-based cooling system to enhance the thermal conductivity and kept the temperature difference as required under different charging and discharging rates. The air-cooled system becomes ineffective at extreme temperature conditions due to their low thermal conductivity and inadequate system design [26]. Liquid-cooled systems are more effective than the air-cooled ones due to their high thermal conductivity. In this context, Qian et al.[27] investigated the effect of the liquid-cooling on the thermal performance of Li-ion battery packs. However, a few types of coolants with dielectric properties can be applied in battery applications.

PCM materials can be used as an alternative solution to traditional cooling systems. The PCM-based cooling method is an effective way to thermally control the battery pack due to their high heat storing-capacity, but low thermal conductivity of PCM is the major limitation for using PCM as a cooling alternative. Li et al.[28] used copper foam as an additive into PCM to enhance the thermal properties of PCM. The thermal properties of this composite solution were analyzed at different pore density of the copper foam. Ettouney et al.[29] studied the enhancement in heat transfer by the addition of metal spheres into PCM.

PCM materials are used in passive cooling systems where they linearly increase their temperature until the phase-change is reached. The employment of PCM stabilizes the temperature during the phase-change, providing a cooling effect because the temperature remains constant during the phase-change. However, the latent heat should be dissipated after the change-phase to not generate a further temperature increase in the battery system.

The basic criteria for the selection of a PCM material for cooling applications are latent heat, thermal conductivity, and temperature range of the phase transition (called "melting phase" in solid-liquid change). These three characteristics regulate the thermal energy storage and release in PCM materials. Regarding the temperature range for the melting point in solid-liquid change, the optimal range of the operating temperature for Li-ion batteries is between 25 and 40°C [2]. However, some scholars highlighted that 25-30 °C is the best temperature range to minimize the aging effect [30]. Rao et al. defined the main characteristics of a PCM material to be used for the heating and cooling of Li-ion batteries [31]:

1. High latent heat, high specific heat, and high thermal conductivity;
2. The melting point in the desired operating temperature range;
3. Little or no sub-cooling during freezing;
4. Small volume changes during phase transition;
5. Stability, non-poisonous, non-flammable and non-explosive;
6. Available in large quantities at a low cost.

2.1 Paraffin wax in thermal management

Paraffin wax is one of the most used PCM materials with a solid-liquid transition[32]. This material consists of a mixture of mostly straight-chain n-alkanes CH3–(CH2)–CH3. The melting temperature can be in the range between 20 to 70 °C. This material is also non-corrosive and chemically inert and stable below 500°C [33]. Moreover, paraffin wax is cost-effective and shows little volume changes on melting and has low vapor pressure in the melting phase [34]. It also provides high latent heat and high specific heat. The thermal storage density ranging from 120 to 210 KJ Kg^{-1}. However, the paraffin waxes have a low thermal conductivity (about 0.2 W $m^{-1}K^{-1}$) [35] which limits their use for battery applications such as automotive [6]. Therefore, to improve thermal management, other solutions and strategies should be considered in the battery design. Many scholars studied the use of additives to define PCM-based composites for increasing thermal conductivity [4].

Table 1 describes the comparison between some relevant scientific papers focused on PCM-based thermal management with solid-liquid solutions. Four papers are focused on battery studies and three are related to solar and photovoltaic systems. Most of them studied the use of metallic foams to increase the thermal conductivity of the pure PCM material such as paraffin wax. The use of metallic foams increases the battery weight; however, the full weight of these battery modules is not shown and often difficult to be calculated by the provided data. Therefore, it is also difficult to estimate the energy density of these batteries solutions. Table 1 reports the column about energy density but this value is calculated without considering the weight of PCM and any other additives because this information was not present in these papers.

Analyzing Table 1, the metallic foams were studied in [28] [36] [37] and [38]. These papers also show that metallic foams enhance the temperature uniformity inside the cells pack. However, this advantage is related to a low porosity value for the analyzed metallic foams. Low porosity is better to increase the thermal conductivity of the PCM-base composites.

Khateeb et al. [36] proposed an aluminum foam with PCM for the thermal management of Li-ion batteries used in electric scooters. A 2-D thermal model was used for analyzing the temperature distribution within the battery module. The use of aluminum foam along with PCM made a significant temperature drop in battery pack along with uniform temperature distribution compared to the case when the only PCM was used for thermal management of battery pack. The type of PCM is not described but the melting range is 41–44 °C and the analyzed reduction in temperature is about 50%. Hussain et al. [37] carried out an experimental study for the thermal management of high powered Li-ion batteries using nickel foam-paraffin composite. This research describes that the use of pure paraffin wax shows a difference of 24% if compared with the PCM composite with copper foam in a battery discharging at a 2-C rate.

Author Accepted Manuscript – Formal publication: https://doi.org/10.1016/j.est.2020.101684

Table 1: Comparison between some relevant scientific papers published in the context of PCM-based thermal management with solid-liquid phase change.

Application	Reference	PCM-based composite and cell type/solar source	PCM type	Results	Energy density in battery module
Electric Vehicle	Khateeb et al.[36], 2005	• Aluminum foam-PCM; • 18650 (2.2 Ah).	Type not available (Melting range: 41–44 °C)	• Temperature drop up to 50%	About 195 Wh/Kg without PCM foam.
	Hussain et al.[37], 2016	• Nickel foam-paraffin wax; • NCR18650B (3.4 Ah).	Paraffin wax (Melting range: 38–41 °C)	• 31% temperature reduction, if compared with air cooling; • 24% temperature reduction, if compared with pure paraffin; • The foam porosity increases the surface temperature of the cells.	About 280 Wh/Kg without PCM foam.
	Li et al. [28], 2014	• Copper foam-paraffin • 18650 (1.5 Ah).	Paraffin RT 44HC (Melting range: 42.76–49.24 °C)	• Uniform temperature distribution • Battery surface temperature decreased with a low porosity of the metal foam	About 76 Wh/Kg without PCM foam
	Wang et al.[38], 2015	• Aluminum foam-paraffin; • Prismatic LiFePO4 cell (16.5 Ah).	Paraffin wax (Melting range: 46–51 °C)	• With foam composite: 28% temperature reduction; • With pure paraffin: 17% temperature reduction; • Aluminum foams improves temperature reduction in discharging.	About 206 Wh/Kg without PCM foam.
Solar Systems	Browne et al.[39], 2015 Browne et al.[40], 2016	• Pure acid eutectic of capric: palmitic; • 500 Wm^{-2}.	Palmitic acid Melting range: 17.72–22.76 °C)	• Heat storage capacity of PV system increases by two times with the use of PCM • The low conductivity of PCM reduce the heat exchanged (the heat released to the hot water)	Data Not available for this application

Photovoltaic Systems	Sharma et al. [41], 2016	• Pure Paraffin wax; • 1000 Wm^{-2}.	Paraffin wax RT42 (Melting range: 38–43 °C)	• Electrical efficiency improvement of 7.7%. • 11.6% temperature reduction using pure paraffin wax	Data Not available for this application

A sandwiched structure with paraffin wax and copper metal foam was studied by Li et al.[28]. The use of such a composite improved the temperature uniformity within the battery pack and also decreases battery surface temperature. Wang et al.[38] investigated the use of a PCM composite paraffin-aluminium foam for improving the temperature distribution within an experimental battery module. The addition of aluminium foam not only enhanced the thermal conductivity of PCM but also improved the temperature uniformity. In this case, a temperature reduction of about 28% has been observed. Anyway, the research also shows the possibility to reduce the maximum temperature upon 17% with the only use of pure paraffin.

Table 1 also reports two papers focused on the thermal management in solar and photovoltaic systems. These works propose the use of pure PCM. While Sharma et al. [41] use the paraffin wax and confirms the possibility to reduce the temperature in electronic applications, Browne et al. [39][40] use the palmitic acid and confirms the limits relates to the thermal exchange after the melting phase of a pure PCM.

Summarizing, past research shows that paraffin, and pure PCM in general, despite having good heat-storing capacity cannot be used alone for the effective thermal management of battery pack or other applications. The use of pure paraffin wax in Li-ion batteries for Electric Vehicle applications have been already investigated in the literature. This seems to give advantages in terms of temperature, but the use of a metallic foam can increase the temperature uniformity with more advantages in the discharging phase at high C-rates of the current [37][38]. The use of additives, such as metallic foams, is one of the ways to improve thermal conductivity. However, the thermal exchange in these composite solutions is related to the metallic porosity. The convective thermal exchange is not considered to improve the cooling of the liquid phase.

This paper highlights the concept of a hybrid integrated thermal management system that incorporates the concept of PCM based cooling along with forced air cooling. This hybrid system is proposed to enhance the thermal performance of a pure PCM based cooling system. A melting phase of around 26–28°C has been investigated despite the past research studied change phases around 40 and 50 °C.

3 Approach

The methodological approach to support the design of a Li-ion battery module is described in Figure 1. The approach is focused on the design of one battery module to be included inside a stacked pack. Generally, modularity is widely used to enhance the assembly of battery packs with many cells. In this paper, the modularization is also extended to the design of the cooling system.

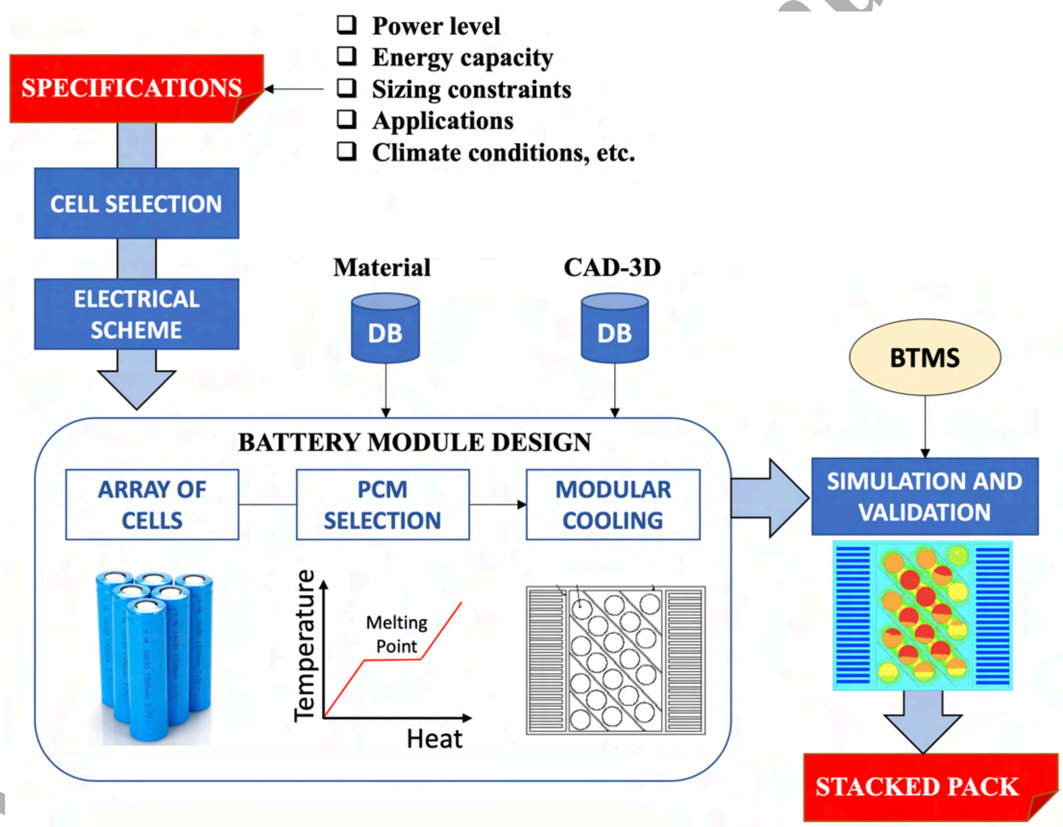

Figure 1: The proposed methodological approach to design a modular battery with cooling.

The requirements related to the applications and the specifications constitute the input of the proposed design process. The selection of cells and their quantity is related to the analysis of the specifications that mainly concerns the power required, the necessary energy capacity, the constraints related to sizing, and the climate conditions to be considered. The design phases, analyzed for the battery module, regard the definition of the arrays of cells, the selection of the PCM material, and the definition of the modular configuration of the cooling system. The definition of the modular cooling system also includes the design of the battery casing. A virtual prototyping analysis is proposed for the early evaluation and validation of the resulting battery module. A CFD (Computational Fluid-dynamics) tool is used for the thermal and fluid dynamics simulations.

Considering the design of one battery module, each module is equal to each other and the number of the employed cells is related to the specific electrical scheme. Therefore, each battery module has an appropriate set of cells which are connected in series/parallels. This electrical scheme can be defined at the beginning of the battery design during the conceptual analysis. The definition of the cell type and the electrical scheme is a task assigned to the electrical engineer. On the other hand, the tasks assigned to the mechanical engineer concern the study of the battery layout, the casing definition, and the cooling analysis.

The novelty of this approach concerns the definition of a cooling system integrated within the modular geometrical layout, as described in Section 4.5. Each battery module has its cooling system which includes a passive solid-liquid PCM unit and a heat exchanger. Moreover, the heat exchanger can regulate the temperature of the PCM system by air-cooling. The integration of a passive PCM cooling and an air-cooling one is controlled by the BTMS during operation. Such a system can regulate the melting point of the PCM filled inside the battery module and maximize efficiency. The blower unit of the air-cooling system is not considered inside the battery module. It is considered as a component of the battery pack and not included in the proposed modular design. The main components of the proposed cooling system for a battery module are:

- **PCM material**: it is filled inside the battery casing while it is in the fluid phase;

- **Sheet-metal plates**: cooling wings wet by the PCM material to maximize the heat exchanged between PCM and the environment;
- **Air-cooling system**: air ducts with heat-exchangers to regulate the temperature inside the battery module;
- **BTMS**: the logic controller which regulates the cooling performance activating the air-cooling system and monitoring the temperature profiles related to the cell zone, PCM material, air, and external conditions.

The presence of an air-cooling system is an opportunity to control the battery's temperature when it exceeds the PCM's melting point. Moreover, the air-cooling system can be also used for heating the battery system in cold conditions when the external temperature is below 0°C. This condition is common in several areas such as North Europe and North America. The proposed cooling combination wants to maximize the benefits related to the use of PCMs by the control and management of the battery's internal temperature in the range of the PCM's melting point. For that reason, the approach proposes the selection of an opportune PCM material with a melting point suitable for its final application considering safety, efficiency, and performance of the specific Li-ion cells (see Section 3.1). The final cooling performance is related to the definition of the PCM material and the sizing of the air-cooling system.

Two databases are considered in the design workflow. The first database is related to the collection of PCM materials to be employed. This database includes information and technical datasheets to support material selection. The second one is a collection of parametric 3D CAD-templates which can be used as a reference Knowledge Base to define the design of a new battery module. This second database includes past-design projects in order to promote the re-use of best practices. The re-use of already validated solutions is important because it can contribute to reducing time and cost related to the design phase of such complex products.

Author Accepted Manuscript – Formal publication: https://doi.org/10.1016/j.est.2020.101684

4 Modeling and test case

This section describes the design of a battery module using the proposed concept of modular design. A 18650-cell has been selected as a basic element for that Li-ion battery. This Li-ion cell has been chosen due to recent market interest for this format which is applied in several applications from electronic and electrical devices to electric vehicles [42].

The specifications of the related Li-ion battery pack concern the design of a 2.4-kWh energy storage unit for stationary applications. Figure 2 describes the assembly of this battery pack. The cooling system includes a passive PCM material and also an air-cooling system to improve the heat exchange. The full battery pack includes 12 200-Wh modules and two plenums for inlet and outlet air flows. The Li-ion modules are connected in parallels and their cells are in series inside each module. Each module can provide a nominal power of 200 W under the condition of 1 C-rate and a peak of 2000 W for a few seconds. Following the modeling and design approaches related to one battery module are described.

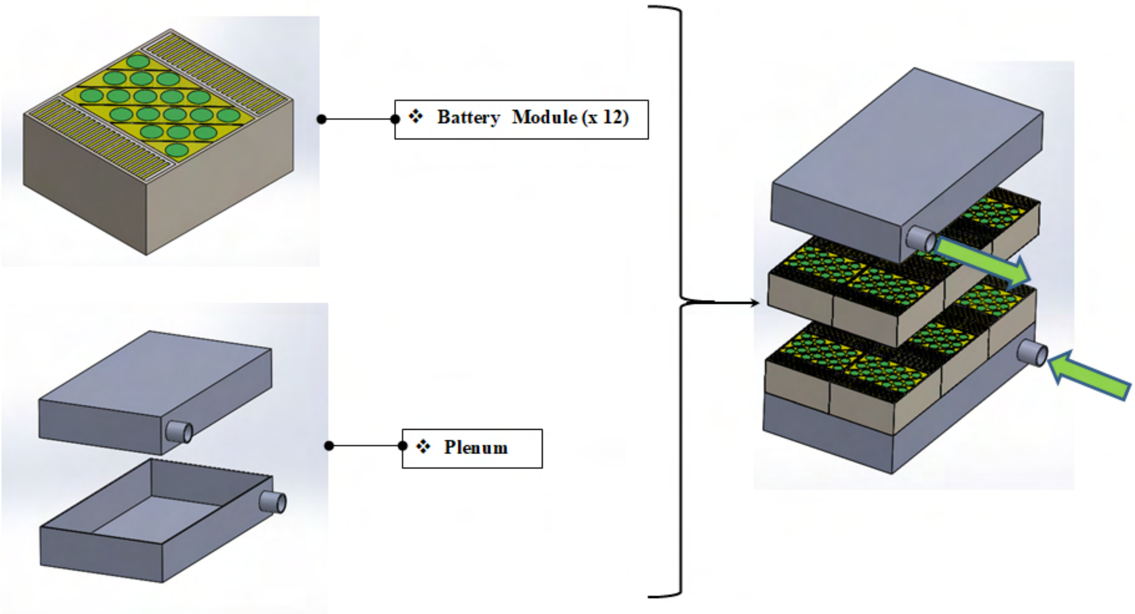

Figure 2: The structure of the modular battery pack.

4.1 Cell data

This study has been focused on the employment of Li-ion 18650 cells with an NMC (lithium-manganese-cobalt-oxide, $LiNiMnCoO_2$) chemistry (Table 2). This type of cell has many advantages such as the small size which is useful for applications with dimensional constraints. These cells also provide good mechanical properties. Their metal casing makes them robust and also acts as a heat sink. Moreover, an internal spiral wound structure separates anode and cathode multiple times increasing the level of safety. Safety characteristics are important in this type of Li-ion cells because they can achieve a high energy density of about 237 Wh kg^{-1}. However, this cell also provides some disadvantages such as low battery capacity and a high-temperature level achieved at high C-rate. In fact, these cells can be discharged at a high current rate (C-rate) such as 10-C. Therefore, temperature monitoring and battery cooling are current topics in this context. The geometrical dimensions of each 18650 cell are 18 mm of diameter and 65 mm of height. Table 4 shows the datasheet related to the 18650 cells used in this paper.

Table 2: Cell datasheet (Model: US18650VTC6).

Property	Value	Unit
Nominal capacity	3000	mAh
Max. continuous discharge current	15	A
Nominal voltage	3.6	V
Discharge end voltage	2.5	V
Charging voltage	4.20	V
Height	65.20	mm
Diameter	18.50	mm
Weight	45.50	g
Lifecycles	300 @0.5C to 80%	cycles

The cathode of the selected Li-ion cell is a combination of nickel-manganese-cobalt. This combination enhances the strengths of each material in the chemical composition. Cobalt increases the battery voltage in Li-ion cells, but it has a high cost [43]. Even if cobalt is an expensive component for Li-ion cells, it provides a value stream in recycling [44]. On the other hand, Nickel is used in NMC cells to its energy density, lower cost, and longer-cycle then simple cobalt-based cells [45].

Heat generation from one cell is due to the electrochemical reactions happening inside its sub-layers such as anode, cathode, and separator. The temperature of a battery pack increases during operation due to the internal heat generation within each Li-ion cell. Therefore, it is necessary to analyze the heat generated by one cell to evaluate the temperature distribution within a battery pack.

4.2 Heat source modeling

This section describes the analytical approach used for computing the heat source generated during the battery operation. The evaluation of the electrochemical heat source focuses on the behavior of one cell. Then, the heat generated by one single cell is extended to each cell of the battery pack during the complete simulation. Therefore, the thermal analysis of one cell is important to further simulate the temperature inside a Li-ion battery pack.

The calculation of the heat generated inside each Li-ion cell depends on three effects: the activation of the interfacial kinetics, the concentration of the species transport, and the Joule heating (Ohm losses). These phenomena concern the movement of particles during the charge and discharge phase, the rates of the electrochemical reactions, and the temperature variation when the Li-ion cell is cycling.

One of the most important studies of the electrochemical and thermal behavior of Li-ion cells was proposed by Bernardi [46], where the heat generated depends on the thermodynamic equilibrium inside the layers of the battery cell (1).

$$\dot{Q_{gen}} = I(V - E_0) - IT\frac{\partial E_0}{\partial T} - \sum_i \Delta H_i^{avg} r_i - \int \sum_j \left(\overline{H}_j - \overline{H}_j^{avg}\right)\frac{\partial c_j}{\partial t}\,dv \quad (1)$$

Equation 1 describes the quantity of heat generated per unit of time inside a Li-ion (evaluated in watt, W). The term *V* represents the variable cell voltage during the charging/discharging phases, E_0 is the opencircuit voltage value (also known with the term *OCV*), *I* is the electrical current applied (>0 in charging and <0 in discharging) and *T* is the temperature of the cell evaluated in kelvin (K). The term ΔH_i^{avg} describes the variation of enthalpy for each *i*-chemical reaction where r_i is the rate of the *i*-reaction; H_j^{avg} represents the partial molar enthalpy of species *j*, and c_j is its concentration [47]. The apex "avg" indicates a property evaluated at the averaged volume concentration. The contribution of the molar enthalpy is calculated over time (*t*) and per the variation of volume (where volume is represented by the term *v*).

Following the assumption proposed by Thomas and Newman [48], this paper considers a simplification of Equation 1 for the heat calculation of one cell. Therefore, only the first two terms of (1) were considered. These terms are important because they represent the exothermic and irreversible heat (2), which is the Joule effect related to the internal resistance (R_i), and the heat due to the entropy changes related to specific reactions (3). This second term can be either endothermic or exothermic in the function of the current and the state of charge (SOC). Moreover, (3) describes the reversible heat and it is related to the ratio $\partial E_0/\partial T$ which is also related to $\Delta S/nF$, where ΔS represents the entropy variation which is divided per the Faraday's constant (*F*) and the number of exchanged electrons (*n*) in the electrochemical reaction.

$$\dot{Q}_{irr} = I(V - E_0) = I^2 R_i \tag{2}$$

$$\dot{Q}_r = IT\frac{\partial E_0}{\partial T} = IT\Delta S\frac{1}{nF} \tag{3}$$

The third and fourth term of (1) are neglected [48] because one depends on side reactions related to aging, which are assumed to be slow enough to be neglected, and the other term is the heat of mixing, which is generated from the formation and relaxation of concentration gradients within the cell. This term can be considered almost zero because the concentration gradients are limited [48]. Considering all these assumptions, (1) was simplified in (4).

$$\dot{Q}_{gen} = Q_{irr+}Q_r = I^2 R_i - IT\Delta S\frac{1}{nF} \tag{4}$$

Author Accepted Manuscript – Formal publication: https://doi.org/10.1016/j.est.2020.101684

The proposed analytical approach aims to calculate the thermal heat generated by a 18650 Li-ion cell considering (4). The output of this calculation is employed inside a CFD tool to simulate the temperature distribution of each cell of the battery module. In particular, (2) and (3) have been implemented inside a user-defined function (UDF) compiled by the CFD tool. This UDF calculates the heat generated on the input current profile and time. Parameters related to the specific 18650 cells have been retried by experimental tests and datasheets. In particular, the internal resistance (*R_i)* and the variation of change in entropy (*ΔS*) with SOC were calculated using experimental tests in a climatic room (Figure 3). The internal resistance was evaluated at a temperature of 20°C, 30°C, and 40°C.

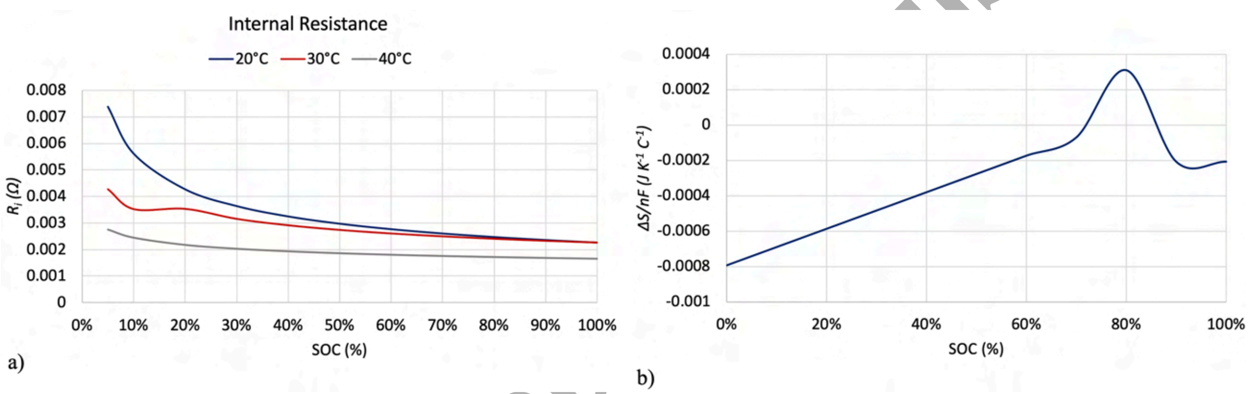

Figure 3: Experimental report with: a) the internal resistance (R_i) and b) the entropy variation evaluated as *ΔS/nF*.

Analyzing the experimental tests reported in Figure 3, the following formulas (5) and (6) have been used for modeling the internal resistance and the entropy variation, which depend on temperature and SOC. These electrochemical equations have been implemented inside a user-defined function to simulate the thermal behavior of one cell by the analysis of a current profile.

$$R_i = \begin{cases} 2.258 \times 10^{-6} SOC^{-0.3952}; \ T = 20°C \\ 1.857 \times 10^{-6} SOC^{-0.2787}; \ T = 30°C \\ 1.659 \times 10^{-6} SOC^{-0.1692}; \ T = 40°C \end{cases} \quad (5)$$

$$\Delta S = \begin{cases} 99.88\, SOC^{-76.67}; & 0 \leq SOC \leq 0.77 \\ +30; & 0.77 < SOC \leq 0.87 \\ -20; & 0.87 < SOC \leq 1 \end{cases} \quad (6)$$

The analytical temperature profile and the experimental values have been compared to validate the thermal output of (4). The result is reported in Table 3. The real data was acquired by cycling a battery cell inside a climate chamber under the temperature of 293 K. The cycled tests are described in Table 3: 0.5-C charge, 0.5-C discharge, 1-C charge, and 1-C discharge. The temperature of the cell was monitored by thermocouples. The test was under the natural convective condition. Equation 7 reports the power balance used to solve the analytical temperature related to this test condition. The convective dissipation and the variation of thermal capacity were added to the formulation described in (4).

$$I^2 R_i - IT\Delta S \frac{1}{nF} = h\left(T_{sup} - T_\infty\right)A + m_{cell} c_{p_{cell}} \frac{dT}{dt} \tag{7}$$

The term h represents the heat convective transfer coefficient (the irradiation aspects have been neglected due to small irradiative area and the temperature differences), the term A is the external surface of one 18650 cell, m_{cell} is the mass of the cell evaluated in kg, and c_p is the specific heat capacity. The term T_∞ represents the temperature of the air inside the climatic chamber. While T is the average internal temperature of the cell, T_{sup} is the superficial temperature involved in the convective and radiative phenomena. The term dT/dt describes the temperature variation inside a cell. Table 3 shows the maximum temperatures achieved at the end of charges and discharges for one 18650 NMC cell tested in the described condition. The table also shows the comparison between analytical and real values. The result confirms the validation of the heat source model because a reduced error has been valuated between analytical and real values.

Table 3: The comparison between analytical and real temperature achieved at the end of charge/discharge phases for an 18650 NMC cell under the condition of natural convective and room at 293 K.

Test	C-rate	h ($Wm^{-2}K^{-1}$) (analytical)	Analytical Max Temperature (K)	Real Max Temperature (K)	Temperature RMS error
Charge	0.5 C	5.35	318	317	0.35
Discharge	0.5 C	5.45	320	319	0.57
Charge	1 C	6.10	338	337	0.38
Discharge	1 C	6.15	340	338	0.58

Author Accepted Manuscript – Formal publication: https://doi.org/10.1016/j.est.2020.101684

The analytical values related to *h*, which is the heat convective transfer coefficient, have been calculated using the following formula (8) where *Nu* is the dimensionless Nusselt number, *λ* is the thermal conductivity of the fluid (W $m^{-1}K^{-1}$), and *L* is the characteristic length of the problem [49].

$$h = {Nu \cdot \lambda}/{L} \tag{8}$$

The *Nu* number has been calculated following the case of external convective heat transfer in vertical cylinders, as described in (9). The term *Pr* and Gr_L are respectively the numbers of Prandtl and Grashof [49].

$$Nu = \left\{ 0.825 + \frac{0.387 \cdot (Pr \cdot Gr_L)^{1/6}}{\left[1 + \left({0.429}/{Pr}\right)^{\frac{9}{16}}\right]^{8/27}} \right\}^2 \tag{9}$$

4.3 PCM modeling

The temperature modeling in PCM materials is defined using Eq. (10) and Eq. (11). While Eq. (10) describes the temperature distribution in PCM, Eq. (11) describes the phase change function (*α*) which indicates the fraction mass of the melted material. The value of *α* is zero when the PCM temperature is less than the melting point and 1 when its temperature exceeds this condition.

$$\rho_m \, C_{p_m} \frac{\partial T}{\partial t} + \rho_m \, C_{p_m} u \cdot \nabla T = \nabla \cdot (\mathrm{k} \nabla T) \tag{10}$$

$$\theta = 1 - \alpha \tag{11}$$

During the phase change, heat conductivity, density and heat capacity change as described in Eq. (12), Eq. (13) and Eq. (14):

$$\rho_m = \theta \, \rho_{phase1} + (1 - \theta) \rho_{phase2} \tag{12}$$

$$C_{p_m} = \frac{1}{\rho_m} \left(\theta \, \rho_{phase1} \, C_{p_{m,phase1}} + (1 - \theta) \rho_{phase2} \, C_{p_{m,phase1}} \right) + L_H \frac{\partial \alpha_m}{\partial T} \tag{13}$$

$$k_{PCM} = \theta\, k_{phase1} + (1-\theta)\, k_{phase2} \tag{14}$$

$$\alpha_m = \frac{1}{2}\frac{(1-\theta)\rho_{phase2} - \theta\rho_{phase1}}{\theta\rho_{phase1} + (1-\theta)\rho_{phase2}} \tag{15}$$

In these equations, L_H is the latent heat, C_{p_m} is the specific heat of the PCM material, ρ_m is the PCM density, k_{PCM} the thermal conductivity, α_m the average phase change function (15), and u is the PCM velocity related to the melted phase. In this paper, as an assumption, the max velocity of the melted phase is 0.008 (m s^{-1}).

In this paper, Paraffin R27 C 21 has been considered as PCM material. Table 4 shows the properties of Paraffin R27 C 21, which is a commercial wax with a transition solid-liquid range between 26 and 28 °C [50] [51].

Table 4: PCM properties for Paraffin R27 C21 [50] [51].

Property	Value
Material name	Paraffin R27 C 21
Melting point (°C)	26-28
Melting point (K)	299-301
Latent heat (kJ kg^{-1})	179
Density liquid (kg m^{-3})	750
Density solid (kg m^{-3})	870
Viscosity (Kg $m^{-1}s^{-1}$)	0.0057933
C_p – Specific Heat (J $Kg^{-1}K^{-1}$)	1950
Thermal Conductivity (W $m^{-1}K^{-1}$)	0.2

Author Accepted Manuscript – Formal publication: https://doi.org/10.1016/j.est.2020.101684

4.4 Battery pack and functional analysis

This section describes the modular approach used to design one battery module. This module has been designed as the smallest unit of a 12-module pack (a matrix of two rows of six modules). Each module is a 54-Volt unit with 18 cells (type 18650 cylindrical NMC) having a nominal capacity of 3000mAh, the nominal voltage of 3.6V and a maximum continuous discharge current of 20A (Table 2).

A functional requirement analysis has been carried out to support the modular design of the proposed Li-ion battery. Table 5 describes the list of the 10 Functional Requirements (FR) which have been defined for the design of this battery pack. Each FR has been assigned to a specific function. Five functions have been highlighted for the design of a Li-ion battery pack: "*Pack Strength*", "*Pack Assembly*", "*Pack Setup*", "*Cells Protection*", "*Battery Efficiency*". The highlighted FRs are related to the mechanical engineering design of the battery pack and include the casing and cooling system.

Table 5: Functional Requirements (FRs) for the design of the battery pack.

FR	Description	Pack Strength	Pack Assembly	Pack Setup	Cells Protection	Battery Efficiency
1	Do not press the cells				x	
2	Increasing temperature exchange (cooling/heating)				x	x
3	Resistance to crash and compression	x			x	
4	Avoid damage for vibration	x				
5	Provide an adequate degree of protection (IP index)				x	
6	Have a reduced sizing		x	x		
7	Reduced number of parts		x			
8	Reduced weight		x	x		
9	Easy to pack			x		
10	Resistance to humidity				x	

Table 6 describes the relationships between each FR. Therefore, this table shows a paired analysis of the FRs. As an example, FR2 is related to the *Cells Protection* function and thereby it has a relation with FR1,

Author Accepted Manuscript – Formal publication: https://doi.org/10.1016/j.est.2020.101684

FR3, FR5, and FR10. Each FR has at least tree interactions with others. The total number of times that each FR is related to others is described in Table 7. Each count is related to rows and columns.

The FRs with more relationships are FR1, FR2, FR3, FR5, and FR10. Following the order of relationships, the main FRs to be considered into the proposed design of the battery pack are: "*Do not press the cells*", "*Resistance to humidity*", "*Provide an adequate degree of protection (IP index)*", "*Increasing temperature exchange (cooling/heating)*", and "*Resistance to crash and compression*"

Following the results of the functional analysis, the battery pack should protect the cells in terms of a crash, collision, and thermal dissipation considering a reduced weight and number of parts. In this test case, the designer has used these requirements to define the layout and structure of the battery's module described in Section 4.5.

Table 6: Relationships between each FR.

FR/FR	1	2	3	4	5	6	7	8	9	10
1		x	x		x					x
2	x				x					x
3	x	x		x	x					x
4			x							
5	x	x	x							x
6							x	x	x	
7						x		x		
8						x	x		x	
9						x	x	x		
10	x	x	x		x					

Table 7: Number of relationships by FR.

FR	Description	Total
1	Do not press the cells	5
2	Increasing temperature exchange (cooling/heating)	4
3	Resistance to crash and compression	4
4	Avoid damage for vibration	3

Author Accepted Manuscript – Formal publication: https://doi.org/10.1016/j.est.2020.101684

5	Provide an adequate degree of protection (IP index)	5
6	Have a reduced sizing	3
7	Reduced number of parts	2
8	Reduced weight	3
9	Easy to pack	3
10	Resistance to humidity	5

4.5 Battery module and modeling

This section describes the design of the battery module. This configuration has been achieved analyzing the results of the functional analysis. In particular, a modular cooling system has been studied and defined to reduce the complexity related to the pack assembly. The cooling system consists of a passive PCM body, which is filled between the battery cells, and an air-flow which regulates the temperature of a finned aluminum heat exchanger, as described in Figure 4. The geometry of the battery module allows each item to be easily stacked and assembled with the air-cooling system. An air-blower unit and plenum-ducts have been evaluated to complete the design of the whole battery pack; however, the design of the battery pack has not been reported in this paper which is focused on the analysis of a single module.

Author Accepted Manuscript – Formal publication: https://doi.org/10.1016/j.est.2020.101684

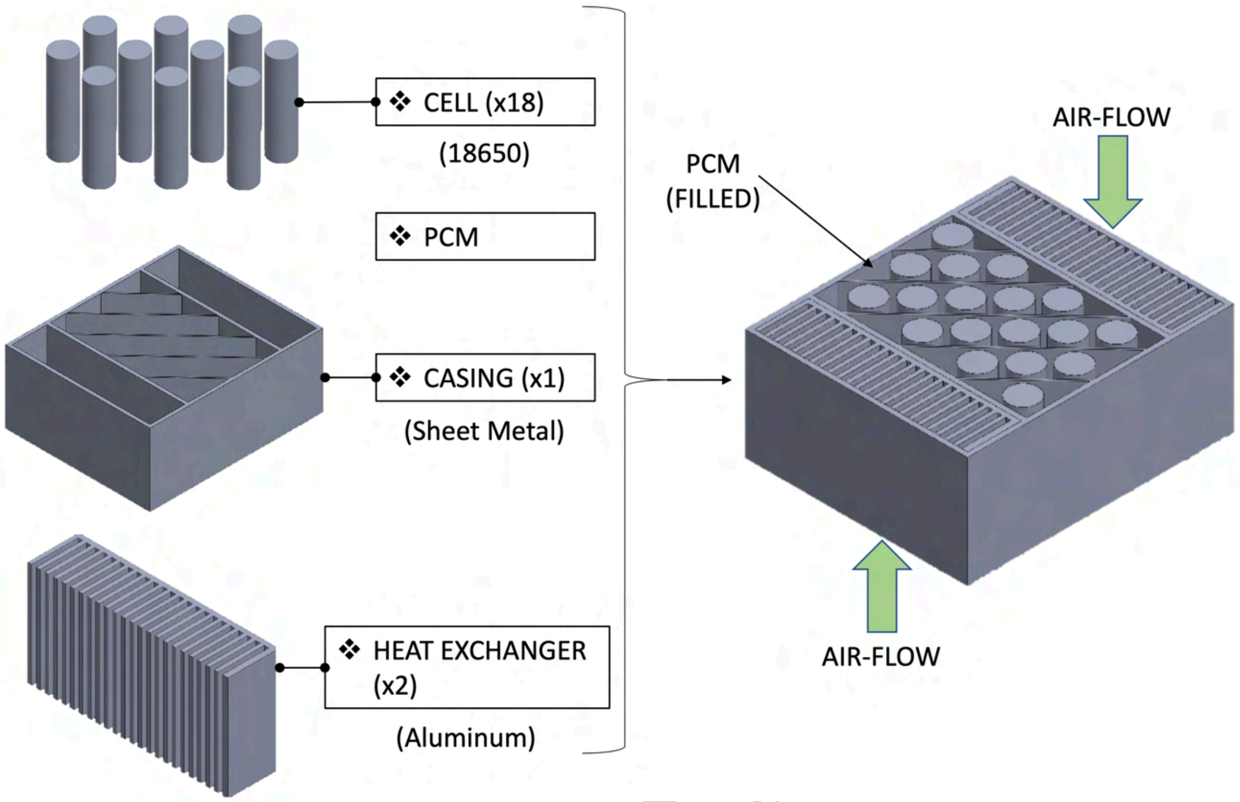

Figure 4: The structure of the proposed battery module with PCM and air-cooling.

Figure 4 describes the assembly and the resulting components of the battery module. The battery module has been defined as a set of 4 components: cell (18 occurrences), PCM (filled inside the cells pocket), casing, and heat exchanger (2 occurrences). This structure shows the following advantages:

- Resistance to vertical compression due to the presence of 11 vertical sheet metal plates;
- Resistance to horizontal crash and vibration due to 5 inclined sheet metal plates and external air-flow channels with heat exchangers;
- Increasing temperature stability of the cells due to the combination of a passive and an air-cooling system. While PCM is a passive system and increases its temperature during operation and after the melting phase, the air-cooling system and the casing conductive can regulate the temperature of the filled PCM and the solid-liquid transition.
- A reduced number of parts involved, if compared with the type of the cooling system and the easy of the pack assembly.

Author Accepted Manuscript – Formal publication: https://doi.org/10.1016/j.est.2020.101684

The array of Li-ion cells is supported by aluminum thin sheets arranged in a diagonal way. This configuration produces structural and thermal advantages. In particular, the thermal advantages are related to the increase of thermal dissipation which is also important in the context of the thermal runaway. While the employment of aluminum reduces the weight of the battery module, the filled PCM increases the weight of the battery module due to the density of the paraffin wax which is 870 kg m^{-3} (in the solid-state). The weight of the paraffin wax, filled in one module, is 0.205 kg (Table 8). Data about the PCM weigh and volume are reported in Table 8.

Table 8: Data about PCM volume and weight.

Parameter	Value
Internal volume	305 cm^3
PCM volume (100% liquid fraction)	274 cm^3
PCM volume (100% solid fraction)	237 cm^3
PCM weight	0.205 kg

The geometrical dimensions of the battery module are length 165 mm x width 135 mm x height 65 mm. CAD software has been used for the parametrical and geometrical modeling of the battery module. A computer Aided Design (CAE) tool has been used to simulate the proposed battery configuration in terms of thermal behavior under specific boundary conditions, as described in Section 5.

4.5.1 Modeling of the sheet thickness

In this section, the sizing of the thickness of the aluminum thin sheets is described. The battery module consists of two types of aluminum sheets: the *external sheet* and the *interior sheet*. While the first one regards the structure of the external case of the analyzed battery module, the second one is the metallic wall surrounded by PCM (as described in Figure 5). The study of the sheet thickness is related to four objectives: the structural behavior, the thermal exchange, the sheet cost, and the sheet weight.

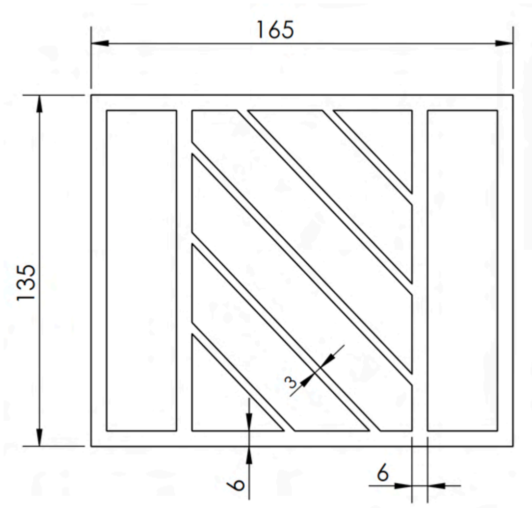

Figure 5: The layout of the aluminum case of the battery module without the Li-ion cells.

The relationship between thickness (*t*) and structural behavior has been analyzed considering the problem of the aluminum sheet as a uniformly loaded rectangular plate with clamped edges and constant thickness. With the assumption of constant material properties, the deflection in the center of the plate (*w*) and the flexural rigidity (D) can be calculated by (16) and (17), as already described in [52].

$$w = \frac{qa^4}{24D} \quad (16)$$

$$D = \frac{Et^3}{12(1-v^2)} \quad (17)$$

The terms *q* represents the uniform pressure loading (expressed in Pa) and *a* is the half-width of the aluminum plate. The loading condition is the pressure generated by the volume change of the PCM material when it achieves 100% of liquid fraction. The aluminum's properties are represented by *E*, which is Young's modulus (Pa), and *v* which is the Poisson's ratio (Table 9). The term *t* is the sheet thickness evaluated in mm.

Table 9: Aluminum properties.

Parameter	Value

Young's modulus, *E*	7 x 10^{10} Pa
Poisson's ratio, *v*	0.33
Thermal conductivity, *λ*	290 W m^{-1} K^{-1}
Density	2700 kg m^{-3}

The loading pressure (*p*) is calculated by analyzing the volume change after the melting phase [47]. Equation (18) and (19) describes the approach for achieving the value of the pressure loading due to the volume change of the PCM material.

$$E_{PCM} = 3(1 - 2v_{PCM})K_{PCM} \quad (18)$$

$$K = -\frac{V_0 \Delta p}{\Delta V} = -\frac{V_0(p - p_0)}{(V - V_0)} \quad (19)$$

Analyzing (18) and (19), the term E_{PCM} is Young's modulus of the PCM material, v_{PCM} and K_{PCM} are the modulus of Poisson and bulk. The max value of the volume change (*ΔV*) is the difference between the volume of the solid-state (V_0) and the liquid condition (*V*). In this calculation, the E_{PCM} is 61.4 MPa [53] and v_{PCM} is 0.37 [54].

The thermal analysis has been also performed to evaluate the relation between the sheet thickness (*t*) and the heat exchange. The heat flux ($\dot{Q}_{sh}$) due to the conduction phenomenon is described by (20) where λ_{al} is the aluminum thermal conductivity, A_{al} is the wall area (m^2), T_M is the melting temperature, T_0 is the external temperature (in the case of external sheet).

$$\dot{Q}_{sh} = \lambda_{al} A_{al} \frac{T_0 - T_M}{t} \quad (20)$$

Figure 6 describes with four graphics the result of the analysis of the relationship between the sheet thickness with the structural behavior, the thermal exchange, the sheet cost, and the sheet weight. The cost has been analyzed with technical catalogues. Using these graphics, a thickness value of 6 mm has

Author Accepted Manuscript – Formal publication: https://doi.org/10.1016/j.est.2020.101684

been chosen for the *external sheet* and 3 mm for the *internal* one. The thickness of 6 mm provides a low deflection in the worst-case scenario (after the melting phase, near the external wall) without compromising the heat flux. A reduced thickness (3 mm) has been selected for the internal sheet because the two sides' compression reduces the structural problems.

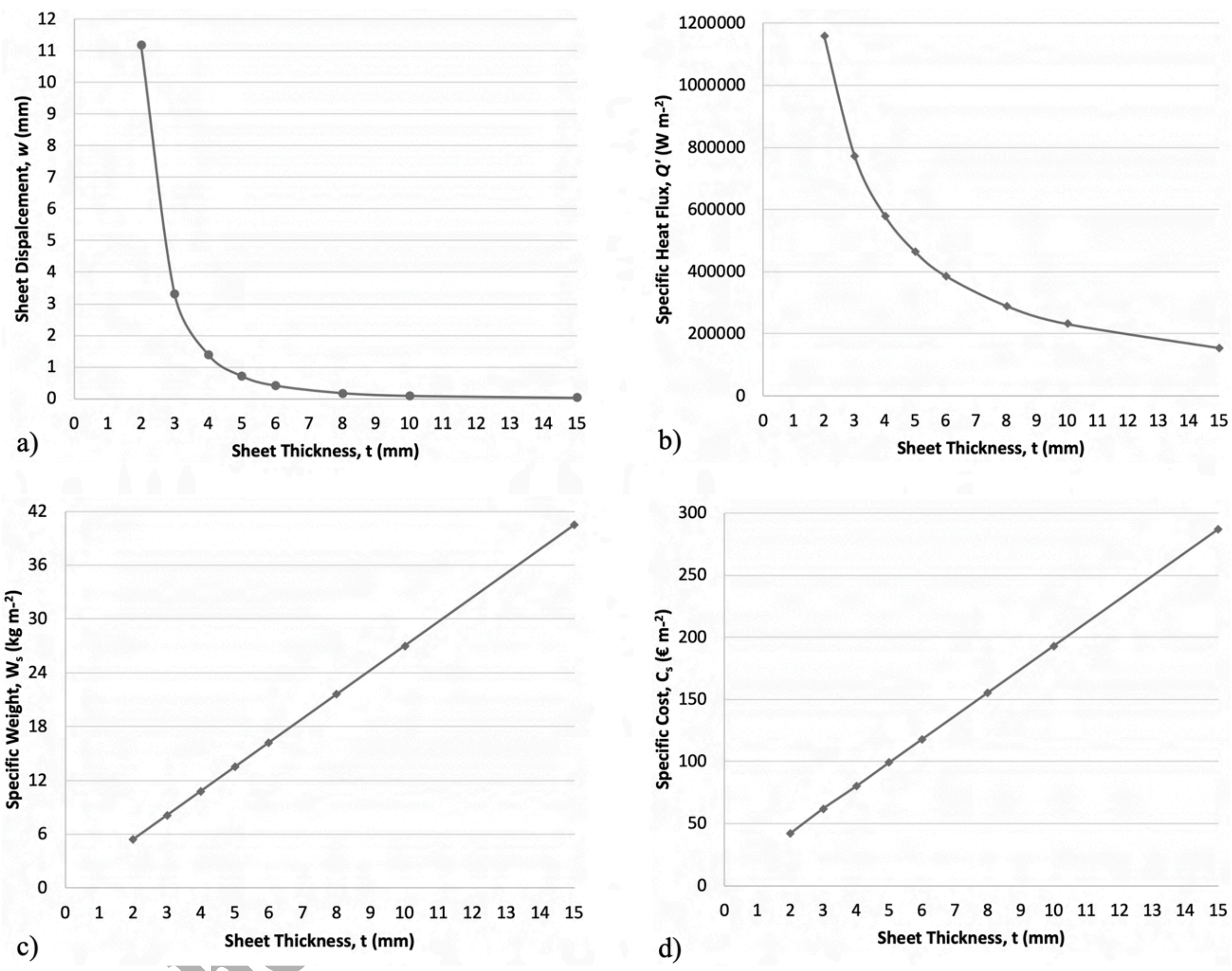

Figure 6: The relationships between the thickness of the external aluminum sheet of the battery module with the sheet displacement under the loading pressure due to the PCM volume change (a), the specific heat flux exchanged by the aluminum wall (b), the specific weight (c), and the specific cost (d).

4.5.2 Modeling of the cell distance

The distance between each cell has been optimized using the balance between the heat exchanged by the PCM layer (Q_{ex}) and the heat stored by the same layer of material ($\dot{Q_{st}}$) in the same time unit. The thickness (t_x) of this layer has been considered as variable in Equation (21) and (22). In these equations,

λ_{PCM} and L_H are the thermal conductivity and the latent heat of the PCM material. The difference between T_M and T_{CM} in (21) is the difference between the PCM melting temperature (26-28 °C) and the maximum cell's temperature (about 65°C).

$$\dot{Q_{ex}} = \lambda_{PCM} A_{PCM} \frac{T_M - T_{CM}}{t_x} \tag{21}$$

$$\dot{Q_{st}} = A_{PCM} t_x L_H \tag{22}$$

Figure 7 describes the trend of Equation (21) and (22) in terms of layer thickness. As described, the value of 3 mm is the optimum point, the balance between the amount of heat exchanged and the heat stored in the PCM layer.

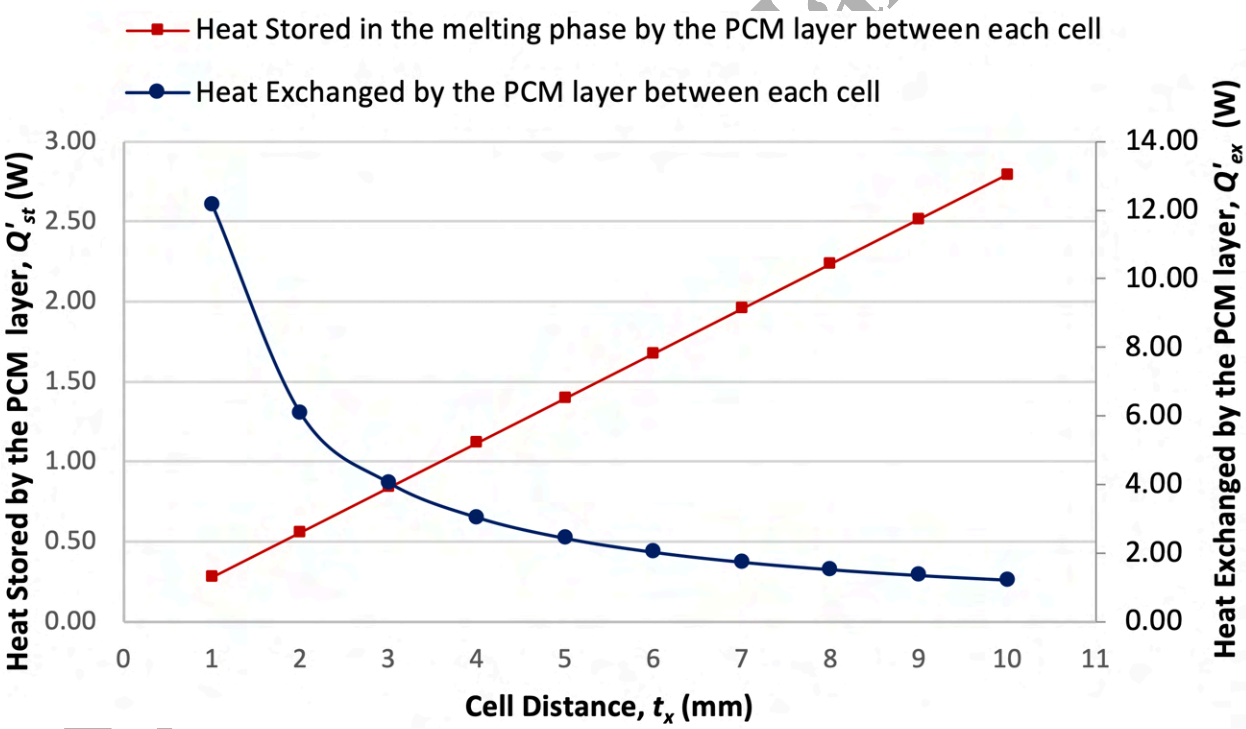

Figure 7: The result of the balance between the amount of heat exchanged and the heat stored in the PCM layer. These two functions are related to the distance between two cells. The red line reports the heat stored in the melting phase by the PCM layer between each cell. The blue line reports the heat exchanged by the same PCM layer between each cell.

4.5.3 Energy density

The energy density of the resulting battery module can be calculated considering the battery capacity (about 200 Wh) and the related weight. Since in the literature this value is sometimes not reported for other papers, there is difficult to provide a comparison with past research. Therefore, here two values of energy density have been calculated. The first value is 69.10 Wh/kg and considers the effective weight of all items. The second one is greater (244.20 Wh/kg) and only considers the weight of the Li-ion cells. This second value has been calculated to compare the analyzed module with other papers that do not report the effective energy density (as seen in Table 1). Table 10 present the data of our work related to the battery's weight, including the weight of each item, and the resultant energy density calculated using both methods with and without considering the weight of PCM, aluminum box, and other items.

Table 10: Data related to the battery's weight and energy density. The value of energy density has been considered with and without the weight of paraffin wax and other items (aluminum box, cables, etc.).

Data	Value
Li-on cells (18 items) - weight	0.819 kg
PCM (paraffin wax) - weight	0.205 kg
Aluminum box - weight	0.550 kg
Heat Exchangers (2 items) - weight	0.820 kg
Cables and PCB controller -weight	0.500 kg
Total battery module's weight	2.894 kg
Energy density (with all items)	69.10 Wh/kg
Energy density without PCM, box, and other items	244.20 Wh/kg

5 RESULTS

Thermal simulations have been carried out using a CAE software tool used for CFD analysis. The results show the thermal behavior at three different operative conditions: discharge at 0.5 C (Section 5.1), discharge at 0.75 C (Section 5.2), and a testing cycle that alternates charge and discharge phases (Section 5.3).

The physical behavior of the PCM material has been modeled in the CFD software. A set of properties has been defined to simulate the phase change during the battery operation. Table 4 describes the properties that have been inserted for modeling the PCM material.

The PCM simulation has been performed considering the energy equation and the solidification and melting models of the CFD software. In this case, two phases (solid and liquid) have been analyzed for the PCM model. The simulations have analyzed the temperature variation and the melt fraction of PCM. As a boundary condition, no melt fraction has been previously defined. As an assumption, PCM was considered full solid at the beginning of the simulation cycle.

The electrochemical heat generated inside each cell has been evaluated using Equation (3), as discussed in Section 4.1. An analytical approach has been defined to solve the thermal problem per each current rate. The resulting values have been settled in the CFD tool as a specific heat thermal source per each cell body. In particular, a User Defined Function (UDF) setting has been used to simulate the testing cycle proposed in Section 5.3. The UDF approach allows the condition of the variable heat source to be reproduced inside the virtual prototyping analysis. The temperature profile and the variation of the liquid fraction in the PCM material have been investigated using the CAE tool in each operative condition. Moreover, the simulations at a constant discharge rate have been also compared to the behavior of the battery module with and without the PCM material.

Author Accepted Manuscript – Formal publication: https://doi.org/10.1016/j.est.2020.101684

5.1 0.5-C discharge

The first simulation activity concerns a 0.5-C discharge comparing the configuration with and without the passive PCM cooling. Both simulation conditions consider a room temperature of 293 K (20 °C) and an air-flow rate of 12 $m^3 h^{-1}$. Figure 8 shows the temperature achieved with and without PCM after a 0.5 C discharge at 100% DOD (Depth of charge). Figure 9 shows a comparison of the related temperature profiles. The maximum temperature achieved is about 324 K (51 °C) without using the passive cooling provided by the PCM material. This temperature level is out of the optimum working range; therefore, continuous operation at this temperature can improve the degradation and depletion of each Li-ion cell. On the other hand, the simulation shows that using a PCM material the cells achieve a maximum temperature of 304 K (31 °C). This configuration can reduce the level of the maximum temperature achieved by up to about 40% for a 100%-DOD discharge at 0.5 C.

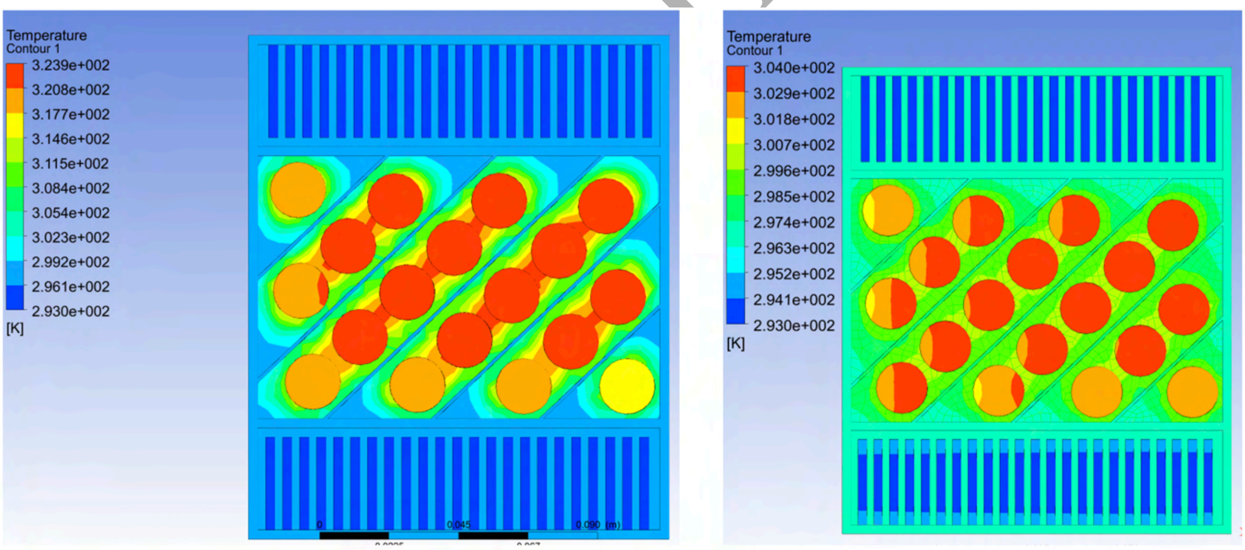

a) b)

Figure 8: The temperature distribution of the battery module after a 0.5 C discharge a) without PCM and b) with PCM.

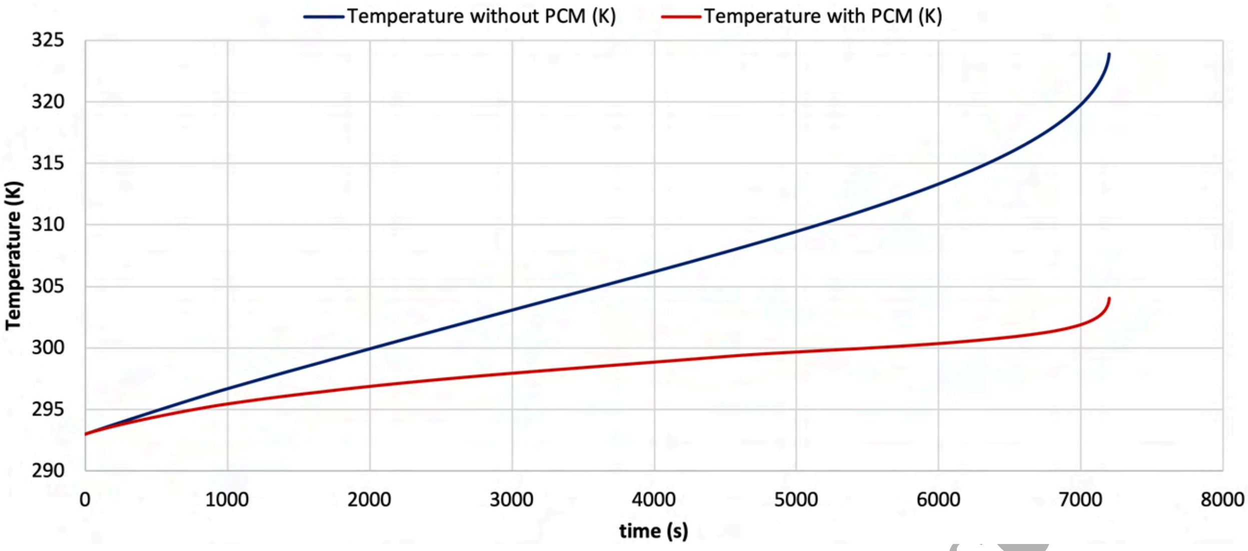

Figure 9: The average temperature profile of the battery module after a 0.5 C discharge without PCM (blue line) and with PCM (red line).

5.2 0.75-C discharge

This second simulation activity regards the battery module discharged in continuous at 0.75 C. In this simulation a comparative analysis has been also proposed between the temperature distribution achieved with and without PCM. The boundary conditions were kept similar to that of 0.5C rate i.e. an air-flow rate of 12 m^3 h^{-1} and 293 K (20 °C) room temperature.

Figure 10 shows the contours related to the temperature distribution within the battery module after discharge at 0.75 C. Figure 11 describes the comparison between the maximum temperature reached within the module when PCM material is employed and not employed. While without PCM the temperature of the maximum cell of the battery module reaches up to 345 K (72 °C), without PCM material the maximum temperature reaches only up to 312 K (39 °C). This configuration can reduce the level of the maximum temperature achieved by up to about 45% for a 100%-DOD discharge at a 0.75-C rate.

Author Accepted Manuscript – Formal publication: https://doi.org/10.1016/j.est.2020.101684

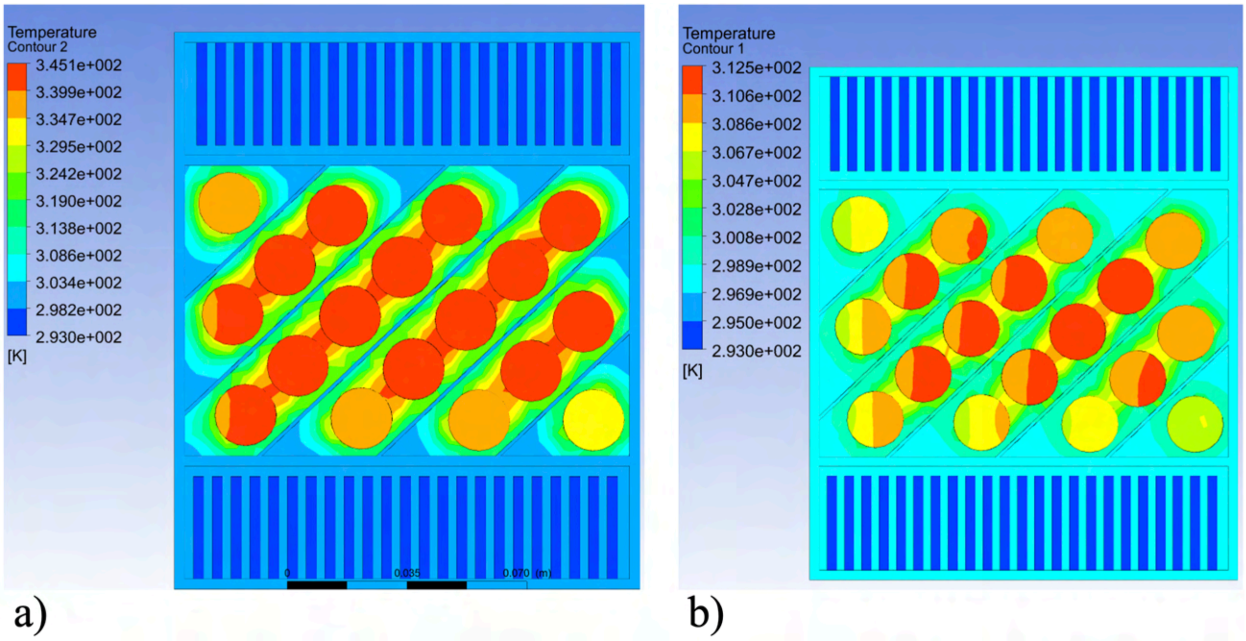

Figure 10: The temperature distribution of the battery module after a 0.75 C discharge a) without PCM and b) with PCM.

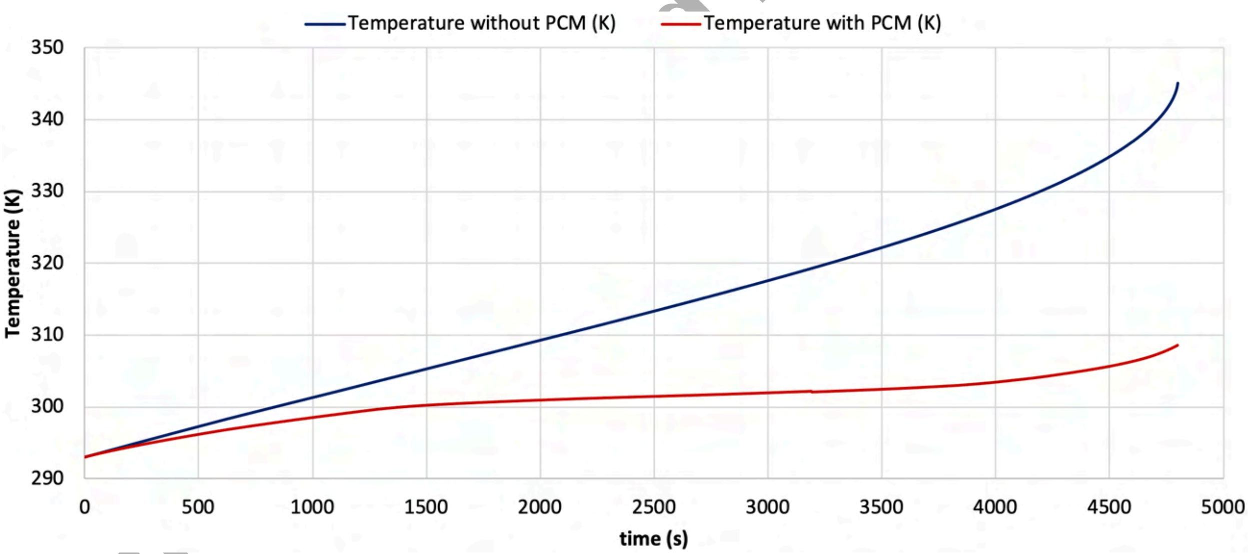

Figure 11: The average temperature profile of the battery module after a 0.75 C discharge without PCM (blue line) and with PCM (red line).

5.3 Testing cycle

This third condition of simulation concerns the testing cycle described in Figure 12. This test is about 3h and 40 min long, it includes different operative steps alternating charge and discharge phases. Figure 13 describes the comparison of the average temperature profile achieved in simulations with and without the PCM material. The condition of the time-depended current was reproduced using a UDF file which includes the data of the current profile and the relative generated heat calculated using Equation (3). This UDF file contains a function which reads the current time of the simulation and assigns the correct value of SOC and current to that time reproducing a real battery test. This procedure was previously validated by experimental tests on one cell. In this simulation, the state of current, voltage, and charge was considered identical to each cell. The calculation of the heat generated in each cell depends on the state of the cell itself and its parameters such as voltage, current, and SOC.

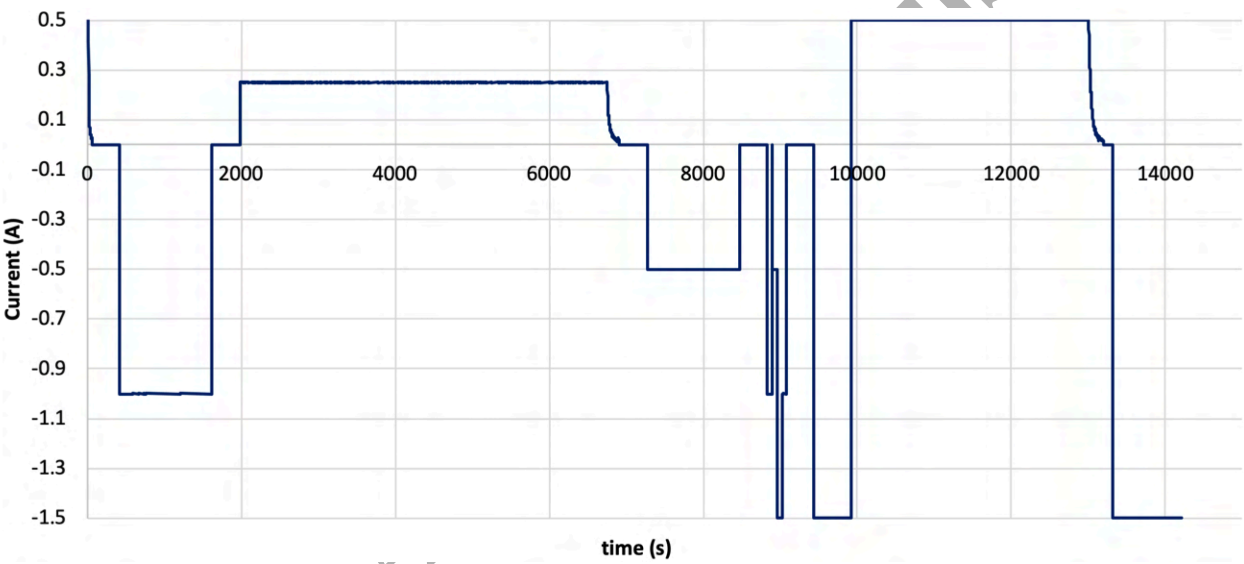

Figure 12: The current profile applied in the testing cycle.

Author Accepted Manuscript – Formal publication: https://doi.org/10.1016/j.est.2020.101684

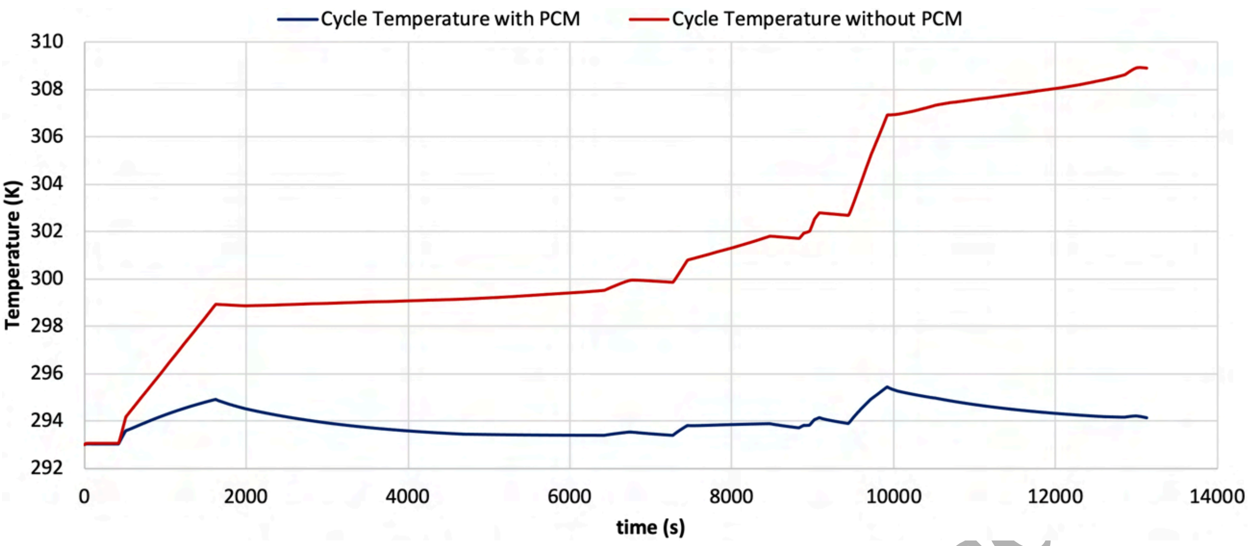

Figure 13: The comparison of the average temperature profile achieved in simulations with and without the PCM material during the testing cycle.

Figure 14 shows the temperature distribution achieved in the battery module at the end of the proposed testing cycle which alternates different phases of charging/discharging. The temperature after the simulations with PCM and air-cooling is about 295 K, which means about 21 °C. In this simulation, the setting of the PCM material and the air-cooling system is able to limit the temperature rising. The maximum temperature peak is about 296 K. Moreover, the temperature of the PCM is under the phase-change condition and the air-cooling system is efficient in heat removal.

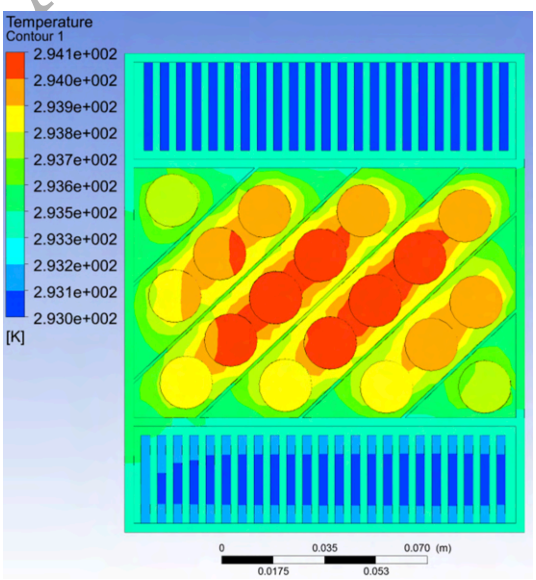

Figure 14: The temperature distribution of the battery module at the end of the analyzed testing cycle.

5.4 Variation of liquid-fraction in PCM

Figure 15 shows the variation of the liquid-fraction in the PCM material during the simulations at 0.5 C and 0.75 C discharge rates. Figure 16 describes the temperature behavior during the solid-liquid transition in both conditions (0.5 C and 0.75 C discharge). Considering the case of 0.5 C discharge, the solid-liquid transition starts at 4500 s which represents about 60% DOD. On the other hand, considering the case of 0.75 C discharge, the solid-liquid transition starts at 1250 s which represents about 26% DOD.

During the 0.75 C discharge, the PCM material is fully liquid when the DOD is about 70% and achieved an increase of about 10 K in the range 70% - 100% DOD. The results also highlight that when the Li-ion module is discharged at 0.5 C rate, the melting of the PCM material achieves the fully liquid phase only at the end of the discharge.

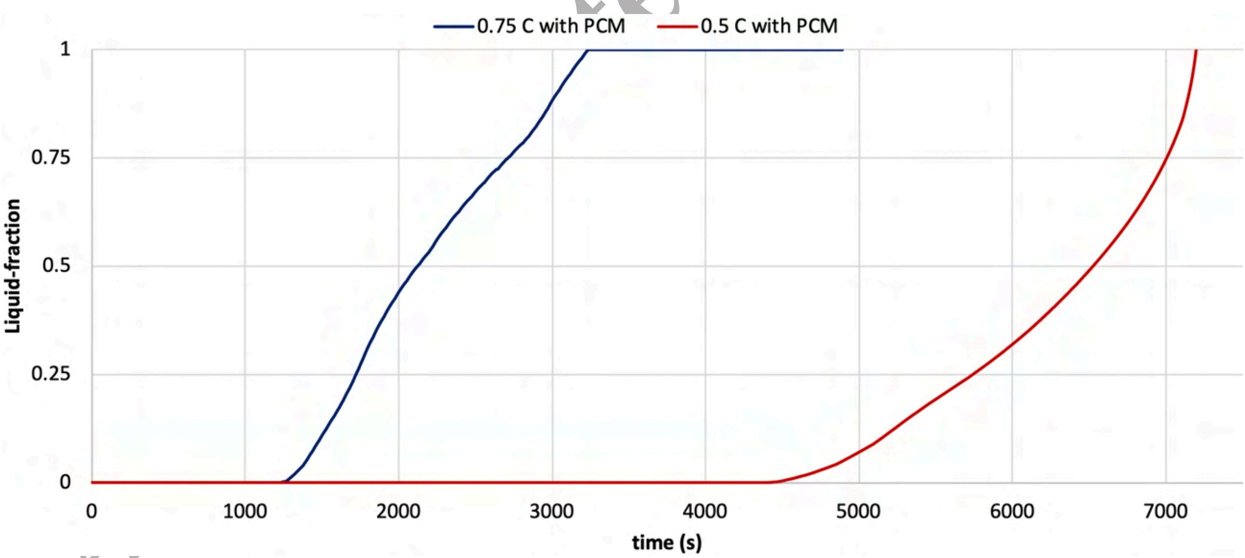

Figure 15: The comparison between a 0.5 C discharge and 0.75 C discharge in terms of liquid-fraction.

Author Accepted Manuscript – Formal publication: https://doi.org/10.1016/j.est.2020.101684

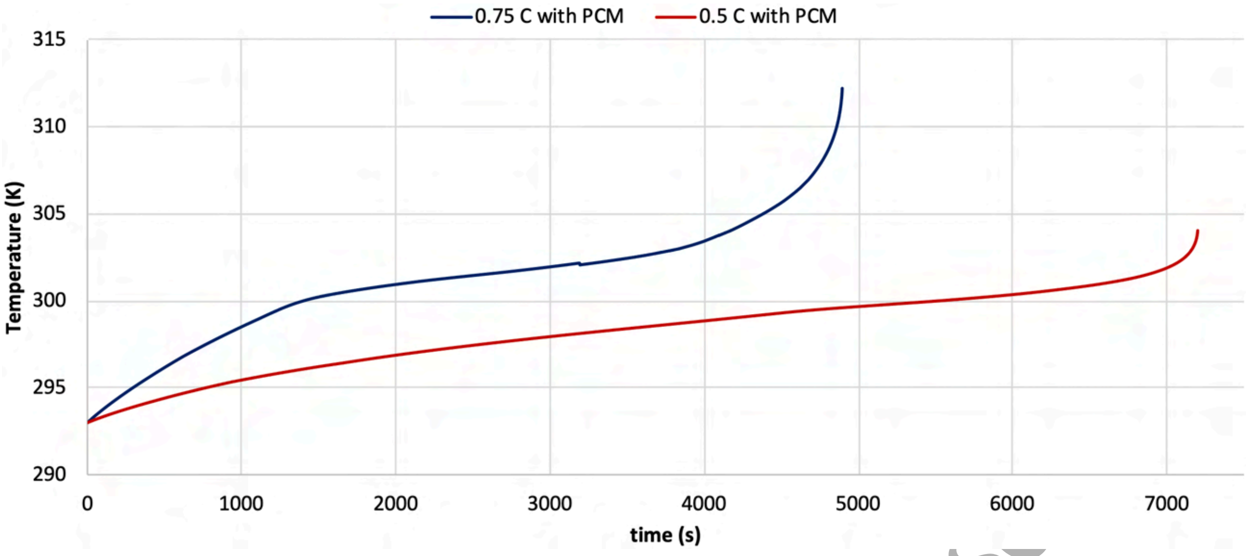

Figure 16: The comparison between a 0.5 C discharge and 0.75 C discharge in terms of the average temperature profile.

6 Discussion

Modularity is an important issue in the design of battery packs. A modular approach can reduce the battery cost and the assembling time during the early design phases. The advantages are the same achieved for conventional configurations products. An important market share of the battery packs is still regarding the niche market for customized solutions in different fields from automotive to smart homes. Therefore, such customized products often require an engineering phase before building. Even if the market of Li-ion batteries differs from the Engineer-to-order sector, the study of a customized battery pack requires a preliminary engineering analysis to confirm the compliant of the electrical performance with the specifications. Moreover, another important analysis concerns the validation of thermal behavior during operation. The thermal analysis is a necessary activity to prevent an excessive temperature level in operation. The achieving of a high-temperature level can increase the aging effect of each Li-ion cell and reduce the battery life, as well known in the literature.

The approach here proposed describes a method to be replicated in the design of Li-ion modules. The method considers an early functional analysis to reduce the gap between functional requirements and battery modularization. The resulting battery's module is defined considering the functional requirements highlighted in the early design phase. This activity is proposed to support a better modularization of the whole battery pack.

The modularity in battery design can be applied both in customized production and mass production. In the context of customized production, this approach can achieve an important target in terms of time reduction in the design activity with benefits on the product cost. Regarding a mass production of batteries, the approach can be also used to optimize the assembling phases in manufacturing.

The test case proposes the study of an 18-cell module with a double cooling system which consists of a PCM material and air-cooling channels with finned heat exchangers. While the first system is a passive cooling system, the second one is an air-cooling system with two heat exchangers. The study considers such a mix of cooling systems to increase the heat exchange and enhance the employment of the paraffin wax as PCM material. During the solid-liquid phase change, paraffin-wax can store an amount of heat until the liquid fraction is 100% of the PCM volume. At this point, it is important to define how to reduce the heat of the PCM system. This paper introduces the air-cooling system to improve the cooling effect of the PCM material avoiding and excessive heat increasing for Li-ion cells when the PCM material is all liquid. When the PCM is liquid, the thermal capacity and the low conductivity make the temperature reduction very difficult to be achieved.

The employed paraffin wax, which is a pure PCM, has low thermal conductivity (0.2 W $m^{-1}K^{-1}$); therefore, the complete melting of this PCM would cause thermal insulation with heat accumulation and thermal runaway risk for each cell. To slow down the melting of PCM, it is possible to increase the cell-to-cell spacing. However, as the cell-to-cell spacing increases, the PCM liquid fraction decreases due to the larger PCM volume. Since an increased cell-to-cell distance would reduce the activation of the PCM material, the distance between each cell has been fixed to 3 mm which is the result of the preliminary analytical optimization described in Section 4.5.2.

In simulations, the battery temperature increases at the end of the discharge phase. The same behavior can be evaluated in charge. This trend is related to the conditions which occur at the end of the discharge (or charge). During the battery cycling, a part of the thermal heat is dissipated by the cooling system, but another part increases the internal cell temperature according to its thermal capacity. The paper has shown an approach to improve the dissipation of heat and reduce the internal temperature of each cell to improve the battery lifespan and efficiency.

In this paper, the use of CFD simulations is proposed to support the designer in the validation of the final configuration of the cooling system. It is well known in the literature that the implementation of CFD tools can reduce the cost related to physical prototyping. However, the proposed approach also aims at reducing time due to trial & error procedures by the introduction of a support methodology for the design of a modular battery pack.

7 Conclusions

A methodological approach is here proposed for the design of battery modules to be stacked in a Li-ion battery pack. The approach has been defined in the context of the customized production of small batches. The design phases concern the arrangement of cells (layout definition), the selection of the PCM material, and the definition of the air-cooling system. The proposed modular approach extends the concept of the functional unit of one module to its cooling system. Therefore, the modularity analysis is extended to the design of the general cooling system for improving the battery assembling.

The proposed cooling system includes a passive PCM method and an air-cooling system for cooling/heating the battery module. Each battery module includes two sides with finned heat-exchangers for improving the air-cooling of the block. Five aluminum plates are defined inside each module to improve the mechanical stiffness and the thermal exchange between PCM and other parts of the system.

The resulting battery module optimizes the cooling performance and the arrangement of the array of cells in terms of thermal management and assembling.

The approach considers the thermal analysis into the early study of the module layout. A CFD simulation activity has been reported to validate the analyzed battery module. The results show the possibility to reduce the maximum temperature of about 40% combining PCM with air-cooling as described in this paper.

REFERENCES:

[1] L. Ianniciello, P. H. Biwolé, and P. Achard, “Electric vehicles batteries thermal management systems employing phase change materials,” Journal of Power Sources, vol. 378, pp. 383–403, Feb. 2018.

[2] R. Koyama, Y. Arai, Y. Yamauchi, S. Takeya, F. Endo, A. Hotta, and R. Ohmura, “Thermophysical properties of trimethylolethane (TME) hydrate as phase change material for cooling lithium-ion battery in electric vehicle,” Journal of Power Sources, vol. 427, pp. 70–76, Jul. 2019.

[3] F. H. Gandoman, J. Jaguemont, S. Goutam, R. Gopalakrishnan, Y. Firouz, T. Kalogiannis, N. Omar, and J. Van Mierlo, “Concept of reliability and safety assessment of lithium-ion batteries in electric vehicles: Basics, progress, and challenges,” Applied Energy, vol. 251, p. 113343, Oct. 2019.

[4] Y. Wei and M. Agelin-Chaab, “Development and experimental analysis of a hybrid cooling concept for electric vehicle battery packs,” Journal of Energy Storage, vol. 25, p. 100906, Oct. 2019.

[5] L. Zhao, Y. Xing, and X. Liu, “Experimental investigation on the thermal management performance of heat sink using low melting point alloy as phase change material,” Renewable Energy, vol. 146, pp. 1578–1587, Feb. 2020.

[6] J. Jaguemont, N. Omar, P. Van den Bossche, and J. Mierlo, “Phase-change materials (PCM) for automotive applications: A review,” Applied Thermal Engineering, vol. 132, pp. 308–320, Mar. 2018.

[7] M. Kenisarin, K. Mahkamov, Solar energy storage using phase change materials, Renew. Sustain. Energy Rev. 11 (9) (2007), 1913-1965.

[8] S. S. Chandel and T. Agarwal, "Review of cooling techniques using phase change materials for enhancing efficiency of photovoltaic power systems," Renewable and Sustainable Energy Reviews, vol. 73, pp. 1342–1351, Jun. 2017.

[9] P. Principi and R. Fioretti, "Thermal analysis of the application of pcm and low emissivity coating in hollow bricks," Energy and Buildings, vol. 51, pp. 131–142, Aug. 2012.

[10] F. Kuznik, D. David, K. Johannes, et al., A review on phase change materials integrated in building walls, Renew. Sustain. Energy Rev. 15 (1) (2011), 379-391.

[11] R. Parameshwaran, S. Kalaiselvam, S. Harikrishnan, and A. Elayaperumal, "Sustainable thermal energy storage technologies for buildings: A review," Renewable and Sustainable Energy Reviews, vol. 16, no. 5, pp. 2394–2433, Jun. 2012.

[12] R. Baetens, B. P. Jelle, and A. Gustavsen, "Phase change materials for building applications: A state-of-the-art review," Energy and Buildings, vol. 42, no. 9, pp. 1361–1368, Sep. 2010.

[13] Á. Á. Pardiñas, M. J. Alonso, R. Diz, K. H. Kvalsvik, and J. Fernández-Seara, "State-of-the-art for the use of phase-change materials in tanks coupled with heat pumps," Energy and Buildings, vol. 140, pp. 28–41, Apr. 2017.

[14] W. Libeer, F. Ramos, C. Newton, M. Alipanahrostami, C. Depcik, X. Li, Two-phase heat and mass transfer of phase change materials in thermal management systems, Int. J. Heat Mass Tran. 100 (2016) 215–223.

[15] A. Acır and M. Emin Canlı, "Investigation of fin application effects on melting time in a latent thermal energy storage system with phase change material (PCM)," Applied Thermal Engineering, vol. 144, pp. 1071–1080, Nov. 2018.

[16] P. Cicconi, L. Postacchini, E. Pallotta, A. Monteriù, M. Prist, M. Bevilacqua, and M. Germani, "A life cycle costing of compacted lithium titanium oxide batteries for industrial applications," Journal of Power Sources, vol. 436, p. 226837, Oct. 2019.

[17] P. Cicconi, M. Germani, D. Landi, and M. Mengarelli, "Virtual Prototyping Approach to Evaluate the Thermal Management of Li-Ion Batteries," 2014 IEEE Vehicle Power and Propulsion Conference (VPPC), Oct. 2014.

[18] M. Lu, X. Zhang, J. Ji, X. Xu, and Y. Zhang, "Research progress on power battery cooling technology for electric vehicles," Journal of Energy Storage, vol. 27, p. 101155, Feb. 2020.

[19] H. Li, C. Liu, A. Saini, Y. Wang, H. Jiang, T. Yang, L. Chen, C. Pan, and H. Shen, "Coupling multi-physics simulation and response surface methodology for the thermal optimization of ternary prismatic lithium-ion battery," Journal of Power Sources, vol. 438, p. 226974, Oct. 2019.

[20] Q. Xia, Z. Wang, Y. Ren, B. Sun, D. Yang, and Q. Feng, "A reliability design method for a lithium-ion battery pack considering the thermal disequilibrium in electric vehicles," Journal of Power Sources, vol. 386, pp. 10–20, May 2018.

[21] P. Cicconi, D. Landi, and M. Germani, "Thermal analysis and simulation of a Li-ion battery pack for a lightweight commercial EV," Applied Energy, vol. 192, pp. 159–177, Apr. 2017.

[22] L. Pelletier, F.-A. LeBel, R. Gonzalez Rubio, M.-A. Roux, and J. P. Trovao, "Design of a High Performance Battery Pack as a Constraint Satisfaction Problem," 2018 IEEE Vehicle Power and Propulsion Conference (VPPC), Aug. 2018.

[23] X. Qian, D. Xuan, X. Zhao, and Z. Shi, "Heat dissipation optimization of lithium-ion battery pack based on neural networks," Applied Thermal Engineering, vol. 162, p. 114289, Nov. 2019.

[24] A.A. Pesaran, "Battery thermal models for hybrid vehicle simulations," *Journal of Power Sources,* vol. 110, issue 2, pp. 377-382, 2002

[25] M. R. Giuliano, A. K. Prasad, and S. G. Advani, "Experimental study of an air-cooled thermal management system for high capacity lithium–titanate batteries," Journal of Power Sources, vol. 216, pp. 345–352, Oct. 2012.

[26] Chen, K., Wu, W., Yuan, F., Chen, L., & Wang, S., "Cooling efficiency improvement of air-cooled battery thermal management system through designing the flow pattern". Energy, 167, 781–790. doi:10.1016/j.energy.2018.11.011

[27] Zhen Qian, Yimin Li, Zhonghao Rao, "Thermal performance of lithium-ion battery thermal management system by using mini-channel cooling," *Energy conversion and Management*

[28] W. Q. Li, Z. G. Qu, Y. L. He, and Y. B. Tao, "Experimental study of a passive thermal management system for high-powered lithium ion batteries using porous metal foam saturated with phase change materials," *Journal of Power Sources,* vol. 255, pp. 9-15, 2014

[29] Ettouney HM, Alatiqi I, Al-Sahali M, Al-Ali SA. "Heat transfer enhancement by metal screens and metal spheres in phase change energy storage systems". Renewable Energy 2004;29:841–60.

[30] S. Landini, J. Leworthy, and T. S. O'Donovan, "A Review of Phase Change Materials for the Thermal Management and Isothermalisation of Lithium-Ion Cells," Journal of Energy Storage, vol. 25, p. 100887, Oct. 2019.

[31] Z. Rao and S. Wang, "A review of power battery thermal energy management," Renewable and Sustainable Energy Reviews, vol. 15, no. 9, pp. 4554–4571, Dec. 2011.

[32] A. Sharma, V. V. Tyagi, C. R. Chen, and D. Buddhi, "Review on thermal energy storage with phase change materials and applications," *Renewable and Sustainable Energy Reviews*, vol. 13, no. 2, pp. 318–345, 2009

[33] S. E. Kalnæs and B. P. Jelle, "Phase change materials and products for building applications: A state-of-the-art review and future research opportunities," Energy and Buildings, vol. 94, pp. 150–176, May 2015.

[34] Sharma A, Tyagi VV, Chen CR, Buddhi D " Review on thermal energy storage with phase change materials and applications," Renewable & Sustainable Energy Reviews, vol. 12, no. 1, pp. 318–45, 2009.

[35] C. R. Abujas, A. Jové, C. Prieto, M. Gallas, and L. F. Cabeza, "Performance comparison of a group of thermal conductivity enhancement methodology in phase change material for thermal storage application," Renewable Energy, vol. 97, pp. 434–443, Nov. 2016.

[36] S. A. Khateeb, S. Amiruddin, M. Farid, J. R. Selman, and S. Al-Hallaj, "Thermal management of Li-ion battery with phase change material for electric scooters: experimental validation," Journal of Power Sources, vol. 142, no. 1–2, pp. 345–353, Mar. 2005.

[37] A. Hussain, C. Y. Tso, and C. Y. H. Chao, "Experimental investigation of a passive thermal management system for high-powered lithium ion batteries using nickel foam-paraffin composite," Energy, vol. 115, pp. 209–218, Nov. 2016.

[38] Z. Wang, Z. Zhang, L. Jia, and L. Yang, "Paraffin and paraffin/aluminum foam composite phase change material heat storage experimental study based on thermal management of Li-ion battery," Applied Thermal Engineering, vol. 78, pp. 428–436, Mar. 2015

[39] M. C. Browne, K. Lawlor, A. Kelly, B. Norton, and S. J. M. Cormack, "Indoor Characterisation of a Photovoltaic/ Thermal Phase Change Material System," Energy Procedia, vol. 70, pp. 163–171, May 2015.

[40] M. C. Browne, D. Quigley, H. R. Hard, S. Gilligan, N. C. C. Ribeiro, N. Almeida, and S. J. McCormack, "Assessing the Thermal Performance of Phase Change Material in a Photovoltaic/Thermal System," Energy Procedia, vol. 91, pp. 113–121, Jun. 2016.

[41] S. Sharma, A. Tahir, K. S. Reddy, and T. K. Mallick, "Performance enhancement of a Building-Integrated Concentrating Photovoltaic system using phase change material," Solar Energy Materials and Solar Cells, vol. 149, pp. 29–39, May 2016.

[42] S. Panchal, M. Mathew, R. Fraser, and M. Fowler, "Electrochemical thermal modeling and experimental measurements of 18650 cylindrical lithium-ion battery during discharge cycle for an EV," Applied Thermal Engineering, vol. 135, pp. 123–132, May 2018.

[43] J. Lim, A. Choi, H. Kim, S. W. Doo, Y. Park, and K. T. Lee, "In situ electrochemical surface modification for high-voltage LiCoO2 in lithium ion batteries," Journal of Power Sources, vol. 426, pp. 162–168, Jun. 2019.

[44] J. L. Sullivan and L. Gaines, "Status of life cycle inventories for batteries," Energy Conversion and Management, vol. 58, pp. 134–148, Jun. 2012.

[45] N. Omar, P. Van den Bossche, G. Mulder, M. Daowd, J. M. Timmermans, J. Van Mierlo, and S. Pauwels, "Assessment of performance of lithium iron phosphate oxide, nickel manganese cobalt oxide and nickel cobalt aluminum oxide based cells for using in plug-in battery electric vehicle applications," 2011 IEEE Vehicle Power and Propulsion Conference, Sep. 2011.

[46] D. Bernardi, E. P., A General Energy Balance for Battery System. Journal of the Electrochemical society, 132, pp. 5-12. (1985).

[47] T. M. Bandhauer, S. Garimella, and T. F. Fuller, "A Critical Review of Thermal Issues in Lithium-Ion Batteries," Journal of The Electrochemical Society, vol. 158, no. 3, p. R1, 2011.

[48] K. E. Thomas, J. Newman, and R. M. Darling, "Mathematical Modeling of Lithium Batteries," Advances in Lithium-Ion Batteries, pp. 345–392, 2002.

[49] Y.A. Cengel, "Introduction To Thermodynamics and heat transfer", McGraw-Hill, 1997.

[50] F. Souayfane, F. Fardoun, and P.-H. Biwole, "Phase change materials (PCM) for cooling applications in buildings: A review," Energy and Buildings, vol. 129, pp. 396–431, Oct. 2016.

[51] M. Thambidurai, K. Panchabikesan, K. M. N, and V. Ramalingam, "Review on phase change material based free cooling of buildings—The way toward sustainability," Journal of Energy Storage, vol. 4, pp. 74–88, Dec. 2015.

[52] E. Imrak and C. Fetvaci, "The Deflection Solution of a Clamped Rectangular Thin Plate Carrying Uniformly Load#," Mechanics Based Design of Structures and Machines, vol. 37, no. 4, pp. 462–474, Oct. 2009.

[53] J. Wang, S. J. Severtson, and A. Stein, "Significant and Concurrent Enhancement of Stiffness, Strength, and Toughness for Paraffin Wax Through Organoclay Addition," Advanced Materials, vol. 18, no. 12, pp. 1585–1588, Jun. 2006.

[54] A. Mann, C. Bürgel, and P. Groche, "A Modeling Strategy for Predicting the Properties of Paraffin Wax Actuators," Actuators, vol. 7, no. 4, p. 81, Nov. 2018.